Frequency-stabilized laser system at 1572 nm for space-borne CO_2 detection LIDAR

Juan Du (杜 娟)[1,2], Yanguang Sun (孙延光)[1], Dijun Chen (陈迪俊)[1,*], Yongji Mu (穆永吉)[1], Minjie Huang (黄敏捷)[1], Zhongguo Yang (杨中国)[1], Jiqiao Liu (刘继桥)[1], Decang Bi (毕德仓)[1], Xia Hou (侯 霞)[1], and Weibiao Chen (陈卫标)[1]

[1]*Key Laboratory of Space Laser Communication and Detection Technology, Shanghai Institute of Fine Mechanics and Optics, Chinese Academy of Sciences, Shanghai 201800, China*

[2]*University of Chinese Academy of Sciences, Beijing 100049, China*

**Corresponding author: djchen@siom.ac.cn*

Received October 24, 2016; accepted December 23, 2016; posted online January 22, 2017

A frequency-stabilized laser system at 1572 nm for space-borne carbon dioxide (CO_2) detection LIDAR to realize the precise measurement of the global atmospheric CO_2 concentration is presented in this Letter. A distributed-feedback laser diode serves as the master laser (ML) and is wavelength locked to the CO_2 line center at 1572.0179 nm using the external frequency modulation technique. The root mean square frequency drift is suppressed to about 50 kHz at an average time of 0.1 s over 8 h. Based on optical phase-locked loops, an online seeder and an offline seeder are offset locked to the reference laser at 1572.024 and 1572.081 nm, respectively, retaining virtually the same frequency stability as the ML.

OCIS codes: 140.3425, 300.6380, 350.6090, 280.1910.

doi: 10.3788/COL201715.031401.

Carbon dioxide (CO_2) measurement is becoming gradually significant to characterize CO_2 sources and sinks, monitor its global budget, and make predictions of future atmospheric compositions[1–4]. Although it has come far, while space-borne passive detection is used generally for CO_2 detection[5,6], this detection technology only operates during the daytime and is impressionable to biases from atmospheric scattering[7,8]. Compared with passive observations, the integrated path differential absorption LIDAR technique that relies on the energy measurement of laser pulse echoes reflected from a hard target has attracted a great deal of attention[7–9]. This LIDAR system emits two single-frequency pulse lasers with different wavelengths: one, called "online," is at the gas absorption line, and the other one, called "offline," is away from the absorption to serve as a radiometric reference. Following the recommendations of preliminary studies, 1572.024 and 1572.081 nm are chosen as the online and offline wavelengths, respectively, according to the minimum sensitivities to errors in water vapor, temperature, ground pressure, scattering surface elevation, and the optimal CO_2 differential absorption[10]. The above two single-mode (SM) pulse lasers are obtained by using an injection-seeded optical parametric oscillator-amplifier system[11–14]. In order to minimize the error contribution from the laser wavelength and to ensure 1 ppm precision for CO_2 measurements, the root mean square (RMS) frequency drift of the online-seeder laser needs to be <0.3 MHz[13]. First, it is necessary to find a suitable absorption line near 1572.024 nm as the frequency reference. Although this is the proverbial wavelength reference for 1.5 μm lasers, for example, C_2H_2 and HCN, even ^{87}Rb does not have strong absorption lines near 1572.024 nm. Therefore, the center wavelength 1572.0179 nm of the R18 CO_2 absorption line is chosen as the absolute wavelength reference. However, the absorption of the 1572.0179 nm line is very weak, so in order to get enough absorption, the length of the reference cell should be very long (typically >10 m). During the last decade, gas-filled hollow-core fibers have been widely investigated and could be used to build the light, compact reference cells[15–17]. But, the surface and high-order modes exhibited in these fibers lead to higher power loss and wavelength-dependent coupling to core modes, causing strong multipath interference (MPI), which limited the frequency stability to the MHz level, which is insufficient for the CO_2 LIDAR application. In addition, these fibers are difficult to splice with standard SM fibers[18]. So, the traditional free-space cell is the only option we have. It must be designed carefully to minimize the MPI and also should be compact and light to fulfill the stringent mass and volume requirements of space-borne equipment. Numata *et al.*[19] achieved a frequency drift of 0.3 MHz at an average time of 0.8 s over 72 h at the 1572.335 nm CO_2 line by using frequency modulation (FM) spectroscopy technology with a bulk cell in 2011. Andreas *et al.*[20] fulfilled a target frequency stability better than 200 kHz at 7 s and below 20 kHz ($<10^{-10}$ fractional stability) at 700 s in terms of the Allan deviation based on an Rb cell and an optical frequency comb (OFC) in 2014. Although the requirement of short-term stability had already been reached, the long-term value was faced with challenges. Gong *et al.*[21] developed a wavelength stabilization method for pulsed difference frequency lasers based on the saturated absorption method combined with two 16 m traditional free-space cells in 2015, but this

method only reached an accuracy of about 30 MHz. Wei *et al.*[22] designed an optical phase-locked loop (OPLL) system to synchronize the frequency and the phase between two external cavity diode lasers, but did not mention the accuracy of the frequency drift.

In this Letter, a frequency-stabilized laser system based on the external FM technique with a bulk cell and OPLLs is presented. One distributed-feedback laser diode (DFB-LD) was frequency locked to the R18 absorption line of CO_2 as the master laser (ML) by using the external FM technology. Another two DFB-LDs were offset locked to the ML as slave lasers (SLs) by using the OPLL. Both the accuracy and stability of the ML were characterized by an analysis of an optical heterodyne beat note with an OFC. The SLs retained virtually the same absolute frequency stability of the ML by analyzing the beat notes between the SLs and the ML.

The absolute frequency locking setup is shown in Fig. 1. A 40 mW SM polarization-maintaining (PM) DFB-LD (FRL15DCWD-A82, FITEL) was used as the ML, with a narrow linewidth of <1 MHz. The tuning coefficients for the current and temperature were 700 MHz/mA and 11.5 GHz/°C, respectively. After going through an isolator, which prevented unwanted feedback from influencing the frequency and linewidth of the laser, the ML output was divided into two parts using a 1:9 PM fiber splitter: 90% of the light was applied to lock this ML, while the rest was used to offset lock the SLs. A fiber-coupler electro-optic modulator (EOM,PM-0K5-10-PFA-PFA, EOSAPCE) driven by a 140 MHz sinusoidal voltage with a modulation index of 3.5 modulated 90% of the light and produced sidebands that were 140 MHz apart around the optical carrier. Subsequently, the modulated laser went across a CO_2 absorption cell with a length of 10 m and a CO_2 pressure of 70 mbar. Finally, an InGaAs photodiode (PD, GD3560, CETC44) detected the transmitted laser beam and generated AC and DC signals. The AC current output of the detector was compared with a local oscillator's signal via a mixer. Then, an error signal in proportional to the laser frequency deviation from the CO_2 line center was produced after a low-pass filter and an amplifier. The appropriate phase delay was chosen to compensate for the unequal delay between the local oscillator and the AC output of the PD. The CO_2 cell pressure, modulation frequency, and depth and the phase shifter delay were optimized to maximize the slope of the error signal. The DC current output of the detector was used to find the absorption peak and switch on the frequency feedback loop automatically by using a digital CPU and other digital circuits. The loop servo fed two signals back to the ML: one was used to find the absorption peak by changing the working temperature, while the other was used to rapidly lock the frequency by adjusting the injection current through a proportion integration (PI) network.

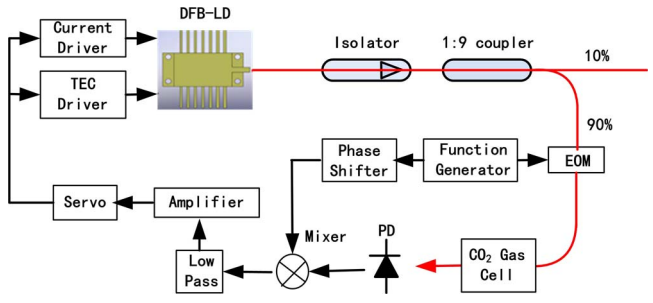

Fig. 1. Absolute frequency locking setup for the ML.

FM technology[23,24] takes advantage of an external phase modulator driven at radio frequency that is large compared to the width of the spectral feature and can effectively decrease the low-frequency noise lying outside the detection bandwidth, but cannot avoid the noise arising from the MPI of a gas cell. So, the minimization of the MPI of a gas cell becomes very important. In our experiment, the CO_2 cell was a homemade astigmatism Herriott cell with a size of $\Phi 100\ \text{mm} \times 80\ \text{mm}$, as shown in Fig. 2(a)[25]. Two astigmatic mirrors were placed inside a chamber filled with CO_2, forming a multipass optical delay line. The adjacent spot spacing on the mirrors was at least 6 times larger than the waist diameter ($1/e^2$), and the reflective number between the two mirrors was 125.

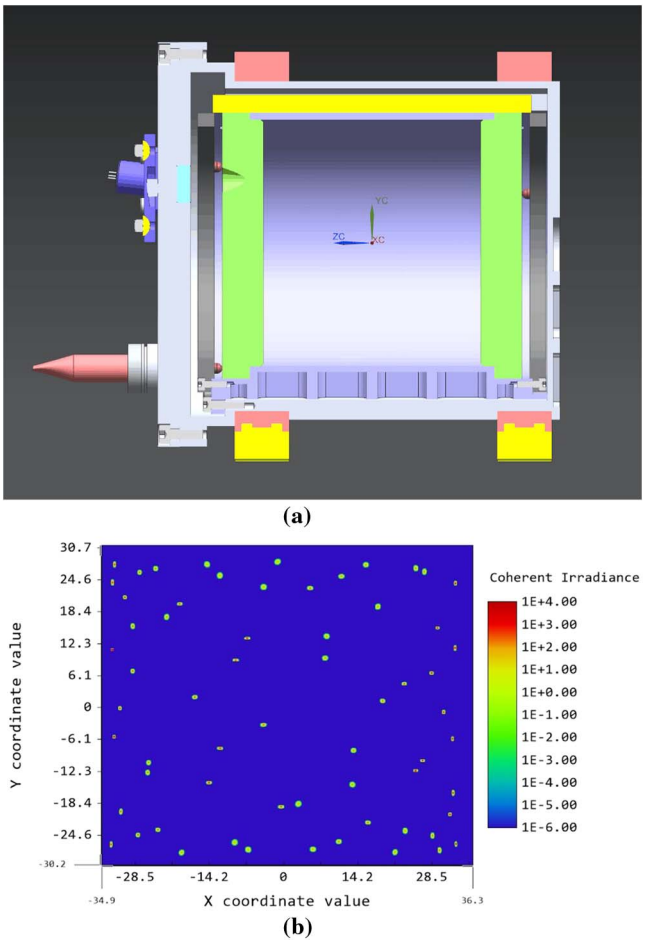

Fig. 2. (a) Profile of the custom-built astigmatism Herriott cell. (b) Space and energy distributions of the light spot of the astigmatism Herriott cell shown in (a).

Figure 2(b) depicts the space and energy distributions of the light spot. This design not only made the construction compact, but also minimized the MPI because of the large spot spacing on the mirrors. The noise of the CO_2 cell was tested as described in Fig. 3(a). The DFB-LD was driven by an LDC3724, which offered a high-stability, low-noise laser control. The output light passed through an isolator and the cell and then was detected by a PD. The signal generator (AFG3252C, Tektronix) output a triangular wave to modulate the current, and, subsequently, the MPI could be detected. Figure 3(b) describes this triangular wave and the signal of the detector. The scanning range of the optical frequency was 2.8 GHz, according to the current coefficient. It also depicts the MPI noise after processing the data, and the maximum noise amplitude and the DC bias voltage were ~2 and ~420 mV, respectively.

According to Ref. [26], a CO_2 reference line is pressure shifted by ~0.22 MHz/mbar in a CO_2 cell. To make sure the RMS of the laser frequency errors was less than 0.3 MHz, the pressure fluctuation should be <1 mbar. That is, to guarantee 8 years of working time, the pressure should be down to 69 mbar. In other words, the leak rate must be lower than 5×10^{-10} Pa · m^3/s. To ensure such a low leak rate, the roughness of the seal contract face was 0.8 μm. Before the installation, all mechanical parts must be cleaned up with an ultrasound, and during the installation, indium was adopted to reduce every gap. Additionally, according to the state equation of ideal gas, the pressure changes 0.235 mbar with a 1°C temperature variation. Therefore, the frequency drift is 0.05 MHz, and the temperature control precision of the CO_2 cell must be lower than 6°C. In this system, a thermoelectric cooler (TEC) was adopted to guarantee the temperature accuracy of the cell was $< \pm1$°C.

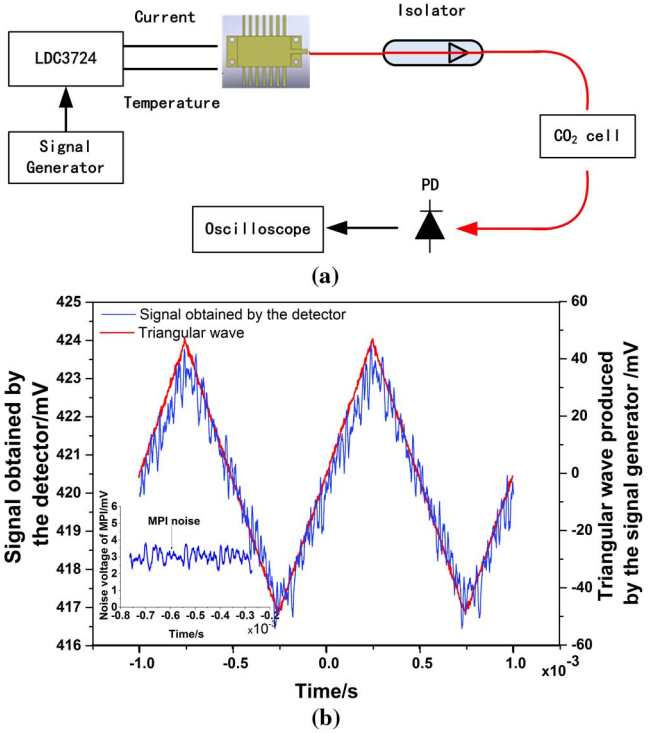

Fig. 3. (a) Schematic of the noise test of the CO_2 cell. (b) Experimental results of CO_2 cell noise test. Detailed MPI noise is also shown, of which the amplitude is about 2 mV.

Figure 4 describes the error signal and absorption peak signal when the ML was scanned by adjusting the working temperature. The error signal afforded a desired linear region near zero with a slope of ~2 mV/MHz. So, the MPI noise, as mentioned above, is obtained in the absorption cell, which is enough to get a 0.3 MHz (RMS) frequency stability.

We measure the frequency deviation from the beat notes between the laser to be detected, and an absolutely stable reference signal is directly necessary, because the error signal could not reflect any frequency deviations caused by the temperature and the mechanism[18]. The output of the ML was combined with the output from an OFC (FC1500-250-WG, MenloSystems) using a fiber coupler. MenloSystems provided this OFC with a 250 MHz comb space, an accuracy of 10^{-14}, and wavelength ranges from 1050 to 2100 nm and 530 to 900 nm. Then, the combined laser output was detected by a highly linear InGaAs PD (DSC30S-HLPD, Discovery). The instantaneous frequency of the beat note from the detector was measured by a frequency counter (Agilent 53220A). Figure 5 shows the frequency stabilization result of the ML, including the details of the beat notes. The frequency drifts of this laser were suppressed to about 50 kHz (RMS) at 0.1 s average time observed over 8 h when it was locked to the 1572.0179 nm CO_2 line. The detailed frequency deviation arising from the MPI is about 150 kHz peak-to-peak, as shown in Fig. 5(b). Figure 5(c) displays the Allan deviation. The frequency stability is better than 5 kHz for a gating time up to 1000 s.

We chose 1572.024 and 1572.081 nm as the wavelengths of the online-seeder and offline-seeder lasers based on the minimum sensitivities to errors in water vapor, temperature, ground pressure, and scattering surface elevation and the optimal CO_2 differential absorption. In order for these two lasers to hold the frequency stability of the ML, the OPLL technology was adopted to stabilize

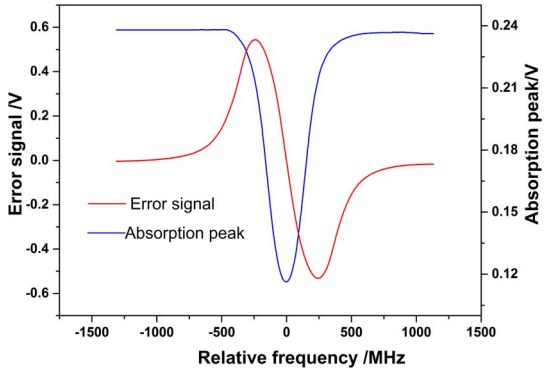

Fig. 4. Relationship between the error signal and the relative frequency.

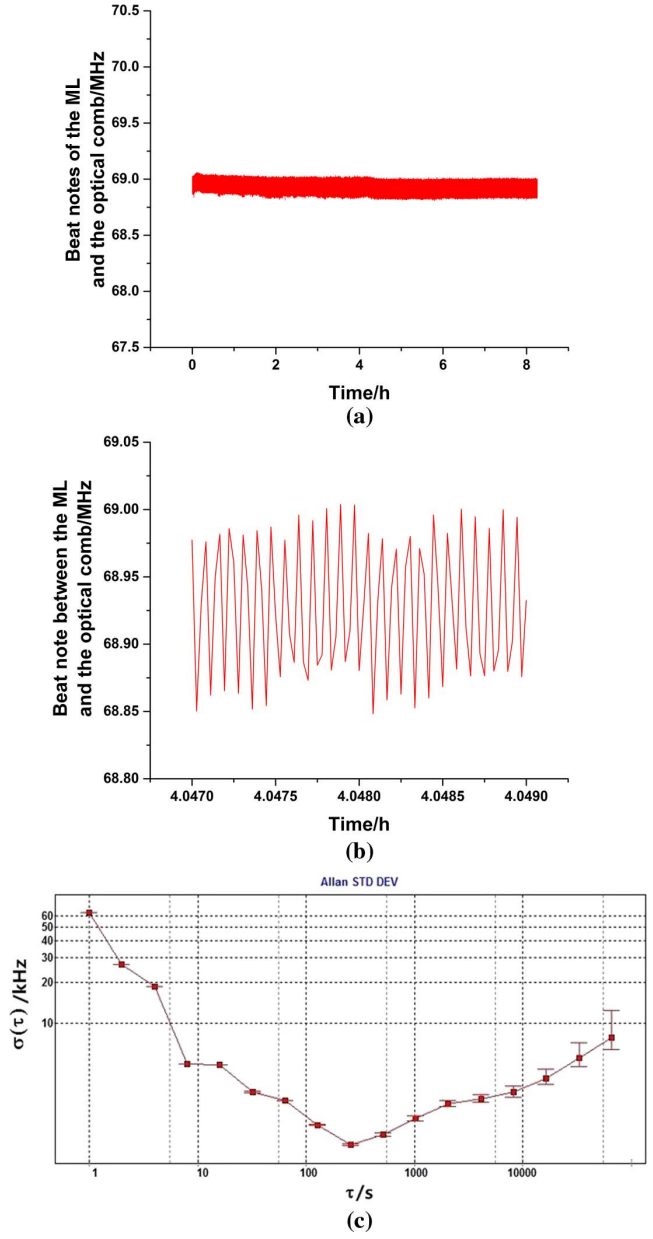

Fig. 5. (a) Frequency stabilization test of the ML. (b) Details of the beat note shown in (a). (c) Allan deviation of the ML.

the relative frequency between the SLs and the ML. The online-seeder and the offline-seeder DFB-LDs were locked with frequency offsets of 760 MHz and 7.616 GHz, respectively, for the 1572.0179 nm ML. The locking setup is shown in Fig. 6. A 1:1 SM PM fiber coupler was used to mix 10% SL power with 5% ML power. Then, the mixed laser output was detected by a 20 GHz PD (DSC40S, Discovery). The produced sinusoidal beat note corresponding to the frequency offset between the online seeder and ML was amplified by a broadband amplifier HEM388E (CETC13) and subsequently frequency divided by a digital frequency divider BW442SM4 (CETC13) by a factor of 8 for 760 MHz, while the beat note between the offline-seeder laser and the ML was amplified by amplifier BW290SM4 (CETC13) and subsequently frequency

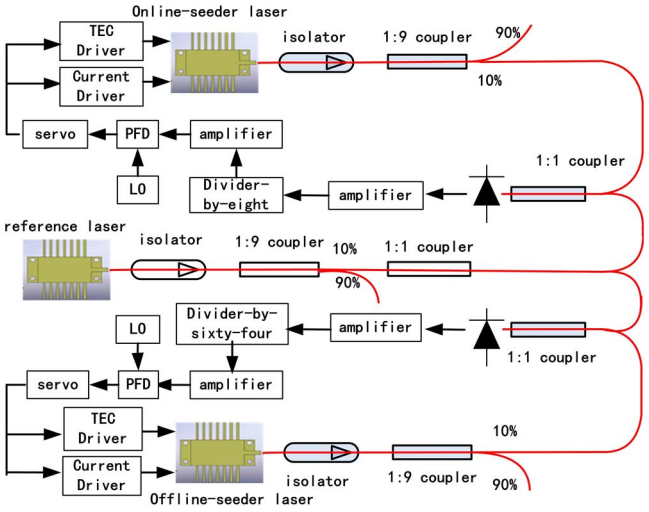

Fig. 6. OPLL system for the offline-seeder laser and online-seeder laser; LO, local signal; PFD, phase-frequency detector.

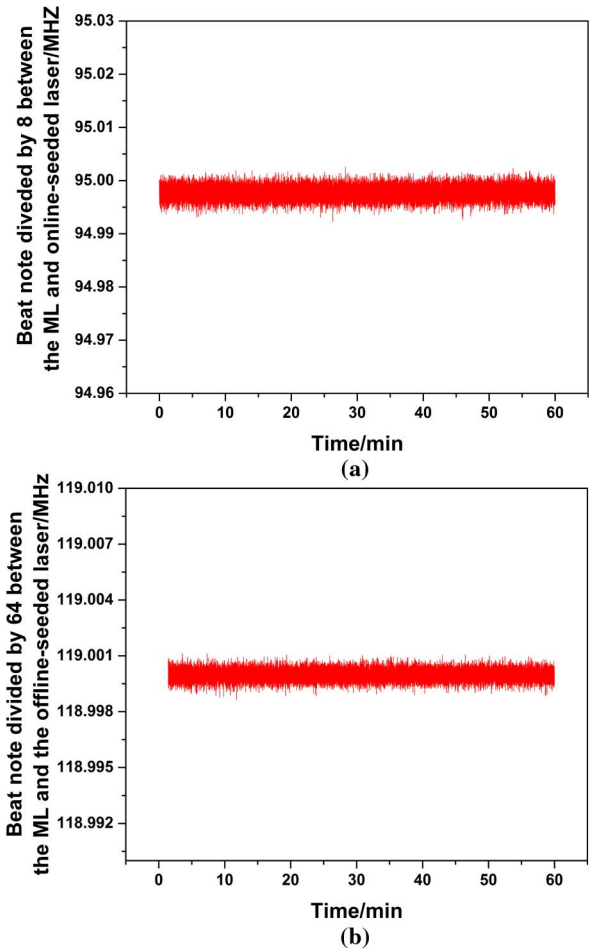

Fig. 7. (a) Frequency drift of online-seeder laser when offset locked to the ML at 760 MHz after being divided by eight using the OPLL setup shown in Fig. 6. (b) Frequency drift of offline-seeder laser when offset locked to the ML at 7.616 GHz after being divided by 64 using the OPLL setup shown in Fig. 6.

divided twice by the same divider BW442SM4 for 7.616 GHz. The divided beat note was amplified again and then input to a digital phase-frequency detector (HMC439, AD), which was used to detect the phase difference between the divided beat note and a precise electronic reference signal generated by a temperature-compensation crystal oscillator. There were two oscillators in the system: one at 92 MHz was used to lock the online-seeder laser, and the other one at 119 MHz was applied to lock the offline-seeder laser. After a loop filter, an error signal proportional to the frequency difference between the two signals was generated. According to the error signal, the analog PI servo controlled the current automatically. The CPU automatically turned on the feedback loop and also monitored the output of the PI to prevent the loop from losing locking.

The divided frequency differences between the SLs and the ML were measured with a frequency counter from Agilent 53220A. As shown in Fig. 7, when offset locked, the RMS value of the fluctuation of the beat note frequency for online-seeder laser was 1.21 kHz and for the offline-seeder laser was 1.45 kHz, so the SLs retained virtually the same absolute frequency stability of the ML. When we convert this fluctuation to the optical frequency for the online laser, it is lower than 60 kHz at 0.1 s average time, and for the offline laser, it is lower than 80 kHz.

In conclusion, in order to ensure 1 ppm precision for CO_2 measurements, a robust laser frequency stabilization system with high-frequency stability is acquired. An ML is wavelength locked to 1572.0179 nm based on an external FM technique, limiting its RMS frequency drift to 50 kHz at 0.1 s average time over 8 h. An online-seeder laser and an offline-seeder laser are offset frequency locked based on the OPLL, stabilizing their absolute frequencies to virtually the same sub-MHz precision as the ML. The stability of this seed laser source is sufficient to satisfy the space-born CO_2 LIDAR requirement. In future, the noise arising from the MPI will be made better with the improvement of the processing craft of the mirror, and the size of cell and the whole system will be made smaller to satisfy researchers' needs in practice.

References

1. J. E. Bauer, W. J. Cai, P. A. Raymond, T. S. Bianchi, C. S. Hopkinson, and P. A. Regnier, Nature **504**, 61 (2013).
2. S. Solomon, *Climate Chang 2007-The Physical Science Basis: Working Group I Contribution to the Fourth Assessment Report of the IPCC* (Cambridge University Press, 2007).
3. I. Y. Fung, S. C. Doney, K. Lindsay, and J. John, Proc. Natl. Acad. Sci. **102**, 11201 (2005).
4. S. Fan, M. Gloor, J. Mahlman, S. Pacala, J. Sarmiento, T. Takahashi, and P. Tans, Science **282**, 442 (1998).
5. N. Saitoh, R. Imasu, Y. Ota, and Y. Niwa, J. Geophys. Res.: Atmos. **114**, D17305 (2009).
6. Atmospheric Infrared Sounder, http://airs.jpl.nasa.gov.
7. J. Caron, Y. Durand, J. L. Bezy, and R. Meynart, Proc. SPIE **7479**, 74790E (2009).
8. J. T. Dobler, F. W. Harrison, E. V. Browell, B. Lin, D. McGregor, S. Kooi, and S. Ismail, Appl. Opt. **52**, 2874 (2013).
9. J. B. Abshire, A. Ramanathan, H. Riris, J. Mao, G. R. Allan, W. E. Hasselbrack, and E. V. Browell, Remote Sens. **6**, 443 (2013).
10. J. Caron and Y. Durand, Appl. Opt. **48**, 5413 (2009).
11. G. Ehret, C. Kiemle, M. Wirth, A. Amediek, A. Fix, and S. Houweling, Appl. Phys. B **90**, 593 (2008).
12. P. F. Ambrico, A. Amodeo, P. Di Girolamo, and N. Spinelli, Appl. Opt. **39**, 6847 (2000).
13. J. Q. Liu, Y. Y. Xie, S. G. Li, H. H. Li, X. H. Ma, and X. L. Zhu, Infrared **2**, 007 (2013).
14. H. Li, X. Zhu, X. Ma, S. Li, and W. Chen, Chin. Opt. Lett. **13**, 111402 (2015).
15. C. Wang, N. V. Wheeler, C. Fourcade-Dutin, M. Grogan, T. D. Bradley, B. R. Washburn, and K. L. Corwin, Appl. Opt. **52**, 5430 (2013).
16. M. Triches, M. Michieletto, J. Hald, J. K. Lyngsø, J. Lægsgaard, and O. Bang, Opt. Express **23**, 11227 (2015).
17. M. Triches, A. Brusch, and J. Hald, Appl. Phys. B **121**, 251 (2015).
18. M. Holá, B. Mikel, J. Hrabina, J. Lazar, and O. Číp, Proc. SPIE **9525**, 95254L (2015).
19. K. Numata, J. R. Chen, S. T. Wu, J. B. Abshire, and M. A. Krainak, Appl. Opt. **50**, 1047 (2011).
20. A. Fix, R. Matthey, A. Amediek, G. Ehret, F. Gruet, C. Kiemle, V. Klein, G. Mileti, J. Pereira do Carmo, and M. Quatrevalet, in *International Conference on Space Optics* (2014).
21. W. Gong, X. Ma, G. Han, C. Xiang, A. Liang, and W. Fu, Opt. Express **23**, 6151 (2015).
22. C. Wei, S. Yan, Aiai Jia, Y. Luo, Q. Hu, and Z. Li, Chin. Opt. Lett. **14**, 051403 (2016).
23. E. D. Black, Am. J. Phys. **69**, 79 (2001).
24. G. C. Bjorklund, Opt. Lett. **5**, 15 (1980).
25. M. Yongji, D. Juan, Y. Zhongguo, S. Yanguang, L. Jiqiao, H. Xia, and C. Weibiao, Appl. Opt. **55**, 7106 (2016).
26. D. Sakaizawa, C. Nagasawa, T. Nagai, M. Abo, Y. Shibata, and M. Nakazato, Jpn. J. Appl. Phys. **47**, 325 (2008).